Self-Adaptive Stabilization Control of a Rotary Pendulum using Nonlinearly-Scaled Model-Reference Gain-Adaptation Law

Omer Saleem*, Fahim Gohar Awan, Samia Mahmood*, Sheroze Liaquat*, Hamza Yousuf***

**Department of Electrical Engineering, National University of Computer and Emerging Sciences, Lahore, Pakistan (e-mail: omer.saleem, samia.mahmood, shahroze.liaquat, hamza.yousuf@nu.edu.pk)*
***Department of Electrical Engineering, University of Engineering and Technology, Lahore, Pakistan (e-mail: fawan@uet.edu.pk)*

Abstract: This article presents the formulation of a novel self-adjusting model-reference-adaptive control law to enhance the position-regulation and disturbance-rejection capability of Rotary-Inverted-Pendulum (RIP) systems. Initially, the baseline Linear-Quadratic-Regulator (LQR) is augmented with a stable online gain-adjustment law that modifies the state-feedback gains online via pre-calibrated state-error dependent dissipative and anti-dissipative functions to improve the system's position-regulation capability. To further enhance the controller's robustness against exogenous disturbances and parametric variations, the baseline LQR is instead retrofitted with the proposed self-adjusting model-reference-adaptive-system that employs Lyapunov theory to formulate a stable online state-feedback gain-adjustment law. The adaptability and flexibility of the model-reference gain-adjustment law is increased by dynamically modifying the adaptation-gains via pre-calibrated Gaussian scaling functions that are driven by the system's state-error variations. The hyper-parameters associated with each control strategy are tuned offline by iteratively minimizing an auxiliary quadratic cost function that captures the state-error and control-input variations. The proposed adaptive control strategies are examined in the physical environment by conducting credible real-time hardware experiments on QNET Rotary Pendulum Board. The experimental outcomes validate the superior reference-tracking and robustness of the proposed adaptive controller even under the influence of exogenous disturbances and modeling-errors.

Keywords: Linear-quadratic-regulator, self-tuning, model-reference-adaptive-controller, Lyapunov theory, Gaussian scaling function, QNET Rotary Pendulum.

1. INTRODUCTION

The Rotary-Inverted-Pendulum (RIP), or Furuta Pendulum, is an inherently unstable system that requires robust-optimal control effort to stabilize itself vertically under the influence of bounded exogenous disturbances (Li et. Al, 2013; Boubaker, 2013). The RIPs are widely favored as a testing platform to examine and validate the efficacy of stabilization control systems designed for under-actuated electro-mechanical systems; such as aircrafts, submarines, aerial robots, missiles, and rockets etc (Bhatti et al., 2015; Zhang et al., 2014). Enhancing the robustness of closed-loop feedback controllers for such under-actuated electro-mechanical systems, to compensate the influence of exogenous disturbances and parametric uncertainties, is a big challenge (Grilti et al., 2018; Saleem et al., 2019a). Extensive research has been done to synthesize optimal stabilization controllers for RIPs (Yu et al., 2008; Mahmoud, 2018). The Linear-Quadratic-Regulator (LQR) is a state-feedback controller that utilizes the nominal state-space model of the RIP system to minimize a quadratic performance index that captures the variations in state-trajectories and control-input to yield optimal control decisions (Sukontanakarn and Parnichkun, 2009; Saleem et al., 2018a). However, despite its optimality, the existence of identification errors and the lack of information regarding the un-modeled intrinsic nonlinearities in the nominal model prevent the LQR from effectively rejecting the external disturbances and load variations (Ghertemani et al., 2011; Prasad et al., 2014). Consequently, the controller's performance gets degraded under parametric-uncertainties which causes the pendulum to collapse. Identification of the time-varying nonlinearities is a difficult task due to the restraints imposed by the system's complex dynamics (Batmani et al., 2017). The stable adaptive control systems are widely favored because of their capability to efficiently mitigate the effects of disturbances caused by random faults, occurring in under-actuated systems, without rendering significant deterioration in the system's overall performance during real-time or mission-critical applications (Saleem at al., 2017; Saleem sta al., 2018b; Saleem et al., 2019b). A well-postulated adaptive system automatically adjusts the critical controller parameters, by using analytical or logical rules, to enhance the system's robustness across a broad range of operating conditions (Szuster and Hendzel, 2017; Bhatti et al., 2018).

The derivative-based auto-tuning mechanisms, and their modified variants, have been extensively used for stable online dynamic adjustment of controller-gains, owing to their quick convergence to local minima (Blanchini et al., 2009; Hanwate et al., 2019). A resilient derivative-based online gain adaptation mechanism has been proposed in (Fisher et al., 2009) to robustify the ship cruise control systems. The "Fisher adaptation mechanism" is composed of dissipative and anti-dissipative terms that significantly enhance the sensitivity of the parameter adjustment law which in turn strengthens the controller's reference-tracking accuracy (Balestrino et al., 2011). However, ill-postulated iterative algorithms inevitably put a recursive computational burden on the embedded processor. The unbounded growth (or decay) of controller gains causes integral wind-up which leads to actuator saturation and possible system failure. The empirical selection of a multitude of hyper-parameters associated with the gain adjustment law is also a laborious task (Balestrino et al., 2011). The Model-Reference-Adaptive-Controller (MRAC) also offers robust control effort to enhance the pendulum's position-regulation accuracy and tolerance against external disturbance (Subramaniana and Elumalai, 2016). It employs Lyapunov theory to analytically formulate a stable derivative-based online gain-adaptation mechanism that directly modifies the state-feedback controller gains, after every sampling interval (Chen, 2017). The Lyapunov function minimizes the difference between the outputs of the reference closed-loop system (governed by the LQR) and the actual closed-loop system to synthesize an asymptotically-stable online gain-adjustment law (Bernat and Stepien, 2012). The pre-fixed adaptation-gains of the gain-adjustment law must be carefully selected as they steer the convergence-rate of state-feedback gains to the local-optimum values, after every sampling interval (Cuong et al., 2013). However, the fixed adaptation-gains fail to address the discontinuities associated with the behavior of RIP system during its equilibrium-state and perturbed-state (Hassanzadeh et al., 2011). Despite the predominantly linear behavior in equilibrium-state, the RIPs encounter undesired limit cycles caused by mechanical friction that severely affects their postural stability. Under the perturbed-state, the intrinsic nonlinearities such as actuator's backlash and force-ripple tend to deteriorate the system's reference tracking performance (Hassanzadeh et al., 2011).

The **novel contribution** of this article is the systematic formulation of a robust nonlinearly-scaled MRAC strategy for an RIP system to enhance its position-regulation accuracy and disturbance-rejection capability. The LQR is used as the baseline control scheme. Initially, the state-feedback gains of the LQR are directly modified online by using the Fisher adaptation mechanism with pre-configured dissipative and anti-dissipative functions (Balestrino et al., 2011). In the next phase, the architecture of the self-tuning regulator is evolved by retrofitting a state-space MRAC with nonlinearly-scaled self-adjusting adaptation-gains. The adaptation-gains are dynamically altered, after every sampling-interval, via pre-calibrated zero-mean Gaussian functions that are driven by the system's state-error variations. This augmentation eliminates the performance limitations rendered by preset adaptation-gains. It increases the controller's degrees-of-freedom which enables the system to quickly and smoothly transit from perturbed-state to equilibrium-state with minimal fluctuations. Additionally, it enhances the adaptability and convergence-rate of the adjusted state-feedback gains which enhances the stabilization controller's robustness against bounded exogenous disturbances. The aforementioned propositions are justified by benchmarking the performance of the proposed nonlinearly-scaled MRAC (N-MRAC) against the fixed-gain LQR as well as "Fisher-adaptive" self-tuning LQR equipped. The comparison is done via credible experiments conducted on the QNET Rotary Pendulum Board (Saleem and Mahmood-ul-Hasan, 2019).

The organization of the rest of the paper is as follows. The experimental setup and its mathematical description are presented in Section 2. The synthesis of baseline LQR is presented in Section 3. The formulation of the proposed state-dependent adaptive controller is presented in Section 4. The experimental evaluation of the proposed controllers is presented in Section 5. The article is concluded in Section 6.

2. SYSTEM DESCRIPTION

The details regarding the hardware setup and mathematical model of the system are presented as follows.

2.1. Experimental Setup

The QNET Rotary Pendulum Board, shown in Figure 1, is used in this research to experimentally examine the efficacy of the proposed control strategies (Ashrafiuon and Whitman, 2011; Balamurugan et al., 2017; Saleem et al., 2020a). The hardware schematic of the system is shown in Figure 2.

Figure 1. QNET Rotary Pendulum Board

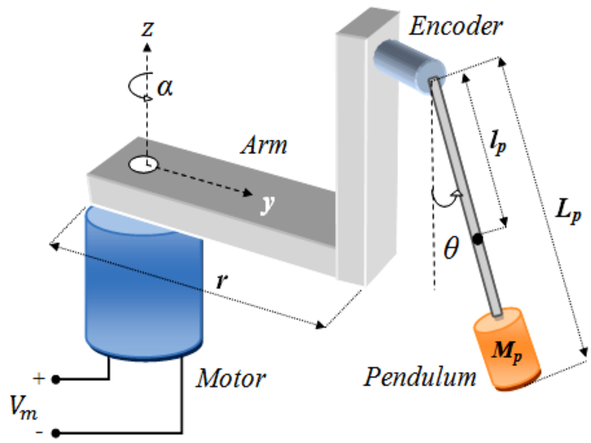

Figure 2. Simplified schematic of RIP

The pendulum rod rotates freely about the y-axis. The pivoted end of the rod is coupled to a rotary encoder that measures the rod's pitch angle, denoted as θ. The rod's free end is coupled with a 0.1 kg counter-mass. The angular motion of the rod depends on the rotation of the arm attached to it. The rod is rotated via a DC geared servo motor. The motor shaft is coupled to an optical encoder that measures the variations in the arm's yaw-angle, denoted as α. The clockwise rotation of the rod and the arm is taken as the positive angular movement about their respective axes. The reference value of θ is fixed at π radians (or 180 degrees), whereas, the initial angular position of the arm's angle, $\alpha(0)$, is selected as the reference value of α. The NI-ELVIS II board is used as a communication relay to exchange the information between the control software and the hardware setup at 9600 bps. The ELVIS board acquires the encoder data at a sampling frequency of 1000 Hz. The acquired data of real-time state-variations is serially transmitted to a LabVIEW-based computer application (Saleem et al., 2020a). The software application is running on a 64-bit, 1.8 GHz embedded computer with 8.0 GB RAM. The application's front-end acts as a graphical user interface that aids in recording and visualizing the instantaneous variations in state-variables. The back-end of the application provides a platform to run the control software routine that receives the digitized sensor readings, generates appropriate torque control signals, and serially transmits the control signals to the hardware setup. It is custom-designed by using the "Block Diagram" tool of the LabVIEW software. The adaptation laws are programmed via C-language codes in the Math-Script tool. The modulated control signals are transmitted to a driver circuit that amplifies them to drive the DC servo motor (Saleem and Mahmood-ul-Hasan, 2019).

2.2. *Mathematical Model*

The Euler-Lagrange technique is adopted to derive the dynamic model of the RIP system (Balamurugan et al., 2017). The difference of the system's total potential energy, V, and kinetic energy, T, is evaluated in terms of the states (φ and θ) and their first-derivatives ($\dot{\varphi}$ and $\dot{\theta}$), to acquire the Lagrangian, L. The expression of L is shown in (1).

$$L = T - V \tag{1}$$

The nonlinear equations associated with the system are obtained as shown below, (Balamurugan et al., 2017).

$$\frac{\delta}{\delta t}\left(\frac{\delta L}{\delta \dot{\varphi}}\right) - \frac{\delta L}{\delta \varphi} = \tau, \qquad \frac{\delta}{\delta t}\left(\frac{\delta L}{\delta \dot{\theta}}\right) - \frac{\delta L}{\delta \theta} = 0 \tag{2}$$

where, τ is the torque applied by DC motor's shaft. In this research, the frictional forces are ignored owing to their negligible effect on the RIP system. The corresponding set of nonlinear equations is presented in (3), (Jian and Yongpeng, 2011).

$$\begin{aligned}\ddot{\varphi} &= -\frac{1}{N}\left(rM_p^2 l_p^2 g(\cos\theta)\theta + J_p M_p r^2(\cos\theta)(\sin\theta)(\dot{\varphi})^2 + \left(J_p + M_p l_p^2\right)\tau\right)\\ \ddot{\theta} &= \frac{1}{N}\left(-M_p l_p\left(M_p r^2(\sin^2\theta)g - J_e g - M_p r^2 g\right)\theta - M_p l_p r(\sin\theta)J_e(\dot{\varphi})^2 \right.\\ &\qquad \left. + M_p l_p r(\cos\theta)\tau\right)\end{aligned} \tag{3}$$

such that, $\tau = \dfrac{K_t(V_m - K_m\dot{\varphi})}{R_m}$

and, $N = J_p\left(M_p r^2(\sin^2\theta) - J_e - M_p r^2\right) - M_p l_p^2 J_e$

These equations are linearized around the point, $\varphi = \theta = \dot{\varphi} = \dot{\theta} = 0$. The following approximations are also used to deal with the small displacements of the rod (Jian and Yongpeng, 2011; Saleem et al., 2020a).

$$\sin\theta \approx \theta, \qquad \cos\theta \approx 1 \tag{4}$$

The state-space model of a linear system is given by (5).

$$\dot{x}(t) = \boldsymbol{A}x(t) + \boldsymbol{B}u(t), \qquad y(t) = \boldsymbol{C}x(t) + \boldsymbol{D}u(t) \tag{5}$$

where, x is the state-vector, y is the output-vector, u is the control input signal, $\boldsymbol{A}$ is the system-matrix, $\boldsymbol{B}$ is the input-matrix, $\boldsymbol{C}$ is the output-matrix, and $\boldsymbol{D}$ is the feed-forward matrix. The state-variables and control input of RIP system used in this research are provided in (6).

$$x(t) = [\alpha(t) \quad \theta(t) \quad \dot{\alpha}(t) \quad \dot{\theta}(t)]^T, \qquad u(t) = V_m(t) \tag{6}$$

where, V_m is the voltage signal applied to the DC motor of the arm. The nominal state-space model of the RIP system is identified by (7), (Saleem Mahmood-ul-Hasan, 2019).

$$\boldsymbol{A} = \begin{bmatrix} 0 & 0 & 1 & 0 \\ 0 & 0 & 0 & 1 \\ 0 & a_1 & a_2 & 0 \\ 0 & a_3 & a_4 & 0 \end{bmatrix}, \qquad \boldsymbol{B} = \begin{bmatrix} 0 \\ 0 \\ b_1 \\ b_2 \end{bmatrix},$$

$$\boldsymbol{C} = \begin{bmatrix} 1 & 0 & 0 & 0 \\ 0 & 1 & 0 & 0 \\ 0 & 0 & 1 & 0 \\ 0 & 0 & 0 & 1 \end{bmatrix}, \qquad \boldsymbol{D} = 0 \tag{7}$$

where,

$$a_1 = \frac{rM_p^2 l_p^2 g}{J_p J_e + J_e l_p^2 M_p + J_p M_p r^2}, a_2 = \frac{-K_t K_m\left(J_p + M_p l_p^2\right)}{\left(J_p J_e + J_e l_p^2 M_p + J_p M_p r^2\right)R_m},$$

$$a_3 = \frac{M_p l_p g\left(J_e + M_p r^2\right)}{J_p J_e + J_e l_p^2 M_p + J_p M_p r^2}, a_4 = \frac{-rM_p l_p K_t K_m}{\left(J_p J_e + J_e l_p^2 M_p + J_p M_p r^2\right)R_m},$$

$$b_1 = \frac{K_t\left(J_p + M_p l_p^2\right)}{\left(J_p J_e + J_e l_p^2 M_p + J_p M_p r^2\right)R_m}, b_2 = \frac{rM_p l_p K_t}{\left(J_p J_e + J_e l_p^2 M_p + J_p M_p r^2\right)R_m}$$

The modeling parameters of the RIP system are identified in Table 1 (Saleem et al., 2020a).

3. BASELINE LINEAR QUADRATIC REGULATOR

The LQR is a model-based state-feedback controller. It utilizes the system's linear state-space model to deliver optimal control decisions by minimizing the deviations in the state-trajectories as well as the control input by using an energy-like quadratic performance index (Lewis et al., 2012). The quadratic performance index is given by (8).

$$J_{lq} = \int_0^\infty \left(x(\tau)^T \boldsymbol{Q} x(\tau) + u(\tau)^T \boldsymbol{R} u(\tau)\right) d\tau \tag{8}$$

Table 1. Identification of RIP system parameter

Symbol	Description	Value
M_p	Mass of pendulum	0.027 kg
l_p	Pendulum center of mass to pivot length	0.153 m
L_p	Length of pendulum rod	0.191 m
r	Length of horizontal arm	0.083 m
J_m	Motor shaft moment of inertia	3×10^{-5} kgm^2
M_{arm}	Mass of arm	0.028 kg
g	Gravitational acceleration	9.810 m/s^2
J_e	Moment of inertia about motor shaft pivot	1.23×10^{-4} kg.m^2
J_p	Moment of inertia about pendulum pivot	1.1×10^{-4} kgm^2
R_m	Motor armature resistance	3.30 Ω
L_m	Motor armature inductance	47.0 mH
K_t	Motor torque constant	0.028 N.m
K_m	Motor back-electromotive force constant	0.028 V/(rad/s)
T_m	Maximum torque	0.14 Nm
V_{rated}	Motor's rated voltage	±24.0 V
I_{rated}	Motor's rated current	5.0 A

where, $\boldsymbol{Q}$ and $\boldsymbol{R}$ are the intermediate-state weighting and control-weighting matrices, respectively. The state-weighting matrix is positive-definite of the form $\boldsymbol{Q} = \boldsymbol{Q^T} \geq 0$. The control-weighting matrix is positive semi-definite of the form $\boldsymbol{R} = \boldsymbol{R^T} > 0$. The optimal control law derived via the LQR approach is given by (9).

$$u(t) = K_{lqr}x(t) \tag{9}$$

such that, $K_{lqr} = -[k_\alpha \quad k_\theta \quad k_{\dot{\alpha}} \quad k_{\dot{\theta}}]$

where, K_{lqr} is the pre-fixed optimal state-feedback gain vector, k_α is the proportional-gain associated with α, k_θ is the proportional-gain associated with θ, $k_{\dot{\alpha}}$ is the derivative-gain associated with $\dot{\alpha}$, and $k_{\dot{\theta}}$ is the derivative-gain associated with $\dot{\theta}$. The gain vector, K_{lqr}, helps in the optimal placement of the system's poles to yield an optimal control effort. The gain vector is evaluated via the expression in (10).

$$K_{lqr} = \boldsymbol{R}^{-1}\boldsymbol{B}^T\boldsymbol{P} \tag{10}$$

where, $\boldsymbol{P}$ is a symmetric positive-definite matrix. The matrix $\boldsymbol{P}$ is evaluated offline by solving the Algebraic Riccati Equation given by (11).

$$\boldsymbol{A^T P} + \boldsymbol{PA} - \boldsymbol{PBR^{-1}B^T P} + \boldsymbol{Q} = 0 \tag{11}$$

Selecting a unique set of state and control weighting-factors is an ill-posed problem (Saleem and Rizwan, 2019). The control-weighting-factor $\boldsymbol{R}$ of J_{lq} is normally selected as unity to economize the overall control-input expenditure. In this research, the coefficients of the state-weighting-matrix $\boldsymbol{Q}$ of J_{lq} are tuned by iteratively minimizing the auxiliary quadratic cost-function, shown in (12), to attain a unique set of weighting-factors that deliver optimum position-regulation accuracy (Saleem et al., 2020a).

$$J_2 = \int_0^\infty \left[\left(e_\alpha(t)\right)^2 + \left(e_\theta(t)\right)^2 + \left(u(t)\right)^2\right] dt \tag{12}$$

where, $e_\theta(t) = \theta(t) - \pi, \quad e_\alpha(t) = \alpha(t) - \alpha(0)$

The physical limitations associated with QNET RIP system, discussed in (Saleem Mahmood-ul-Hasan, 2019), are also taken into account while refining the selected weighting factors of J_{lq}.

- **Rod regulation:** $|e_\theta(t)| < 0.35$ rad.
- **Arm regulation:** $|e_\alpha(t)| < 2.97$ rad.
- **Control input limit:** $|V_m(t)| < 20.0$ V.

The range of values of e_θ, e_α, and V_m defined in the criterion above are experimentally identified. Owing to the pendulum dynamics, the rod collapses if e_θ exceeds the defined range. Similarly, if e_α violates the defined range, the power-chord and data-cable of the rotary encoder coupled with the rod's pivot obstruct the rotational movement of the arm causing the rod to collapse. The control input is kept within ±20.0 V to avoid over-heating or unnecessary wear-and-tear of the motor's winding. The RIP is erected manually and the weighting-factors are calibrated iteratively until the desired performance objectives are achieved. The optimized weighting-matrices used in this research are given by (13).

$$\boldsymbol{Q} = \begin{bmatrix} 38.2 & 0 & 0 & 0 \\ 0 & 52.6 & 0 & 0 \\ 0 & 0 & 5.3 & 0 \\ 0 & 0 & 0 & 2.1 \end{bmatrix}, \quad \boldsymbol{R} = 1 \tag{13}$$

The gain vector, K_{lqr}, is calculated offline as shown below.

$$K_{lqr} = [-6.21 \quad 130.56 \quad -4.22 \quad 17.83] \tag{14}$$

4. SELF-ADAPTIVE CONTROL SYSTEM DESIGN

The online gain-adjustment enhances the system's immunity against bounded disturbances as well as its reference tracking accuracy. This section presents the detailed design procedure of two self-adaptive multivariable control strategies.

4.1. Fisher-adaptive Self-tuning Regulator (F-STR)

The process of online gain-adaptation is initiated by employing the "Fisher" adaptation mechanism with pre-calibrated dissipative and anti-dissipative functions (Fisher et al., 2009). It flexibly modifies the controller's state-feedback gains online which enable the controller to respond to a wide range of operating conditions in practical under-actuated systems (Balestrino et al., 2011). The Fisher-inspired adaptation law does not require a priori knowledge of the system's model. Instead, it initiates from the nominal preset values of gains and then iteratively modify them online on the basis of real-time state-error variations. The adaptation functions used in this research are expressed as follows (Balestrino et al., 2011).

$$\dot{k_\alpha}(t) = -\gamma_\alpha . k_\alpha(t) + \beta_\alpha . |e_\alpha(t)|^2 \quad (15)$$

$$\dot{k_\theta}(t) = -\gamma_\theta . k_\theta(t) + \beta_\theta . |e_\theta(t)|^2 \quad (16)$$

$$\dot{k_{\dot{\alpha}}}(t) = -\gamma_{\dot{\alpha}} . k_{\dot{\alpha}}(t) + \beta_{\dot{\alpha}} . \left(e_\alpha(t) . \dot{e}_\alpha(t)\right) \quad (17)$$

$$\dot{k_{\dot{\theta}}}(t) = -\gamma_{\dot{\theta}} . k_{\dot{\theta}}(t) + \beta_{\dot{\theta}} . \left(e_\theta(t) . \dot{e}_\theta(t)\right) \quad (18)$$

where, γ_x and β_x are decay-rates and inflation-rates, respectively. The *dissipative* parts of these functions are represented by $-\gamma_x . k_x(t)$. They decrease the rate-of-change of the corresponding gain exponentially with the decay-rate γ_x under low error conditions in order to damp the oscillations and minimize control energy consumption. It also prevents the integral wind-up. The *anti-dissipative* parts are represented by $\beta_x . |e_x(t)|^2$ or $\beta_x . e_x(t) . \dot{e}_x(t)$. They enlarge the corresponding gains under large error conditions, and vice-versa, to manipulate the stiffness or softness of control effort as the response diverges or converges towards the reference, respectively (Balestrino et al., 2011). The adaptive functions can be represented in the form of a first-order differential-equation as shown in (19).

$$\dot{K}_f(t) = -\boldsymbol{F} K_f(t) + \boldsymbol{G} v(t) \quad (19)$$

such that, $K_f(t) = \begin{bmatrix} k_\alpha(t) \\ k_\beta(t) \\ k_{\dot{\alpha}}(t) \\ k_{\dot{\theta}}(t) \end{bmatrix}$, $\boldsymbol{F} = \begin{bmatrix} \gamma_\alpha & 0 & 0 & 0 \\ 0 & \gamma_\theta & 0 & 0 \\ 0 & 0 & \gamma_{\dot{\alpha}} & 0 \\ 0 & 0 & 0 & \gamma_{\dot{\theta}} \end{bmatrix}$,

$\boldsymbol{G} = \begin{bmatrix} \beta_\alpha & 0 & 0 & 0 \\ 0 & \beta_\theta & 0 & 0 \\ 0 & 0 & \beta_{\dot{\alpha}} & 0 \\ 0 & 0 & 0 & \beta_{\dot{\theta}} \end{bmatrix}$, $v(t) = \begin{bmatrix} |e_\alpha(t)|^2 \\ |e_\theta(t)|^2 \\ e_\alpha(t) . \dot{e}_\alpha(t) \\ e_\theta(t) . \dot{e}_\theta(t) \end{bmatrix}$

where, $K_f(t)$ is a vector containing the time-varying state-feedback gains $k_x(t)$, $v(t)$ is a vector containing the corresponding error-dependent terms used in each function, $\boldsymbol{F}$ is a positive definite matrix containing the decay-rates, γ_x, and $\boldsymbol{G}$ is a positive definite matrix containing the inflation-rates, β_x. The positive constants, γ_x and β_x, are carefully selected to prevent indefinite increment (or decrement) in the gains under long-drifting disturbances which generally lead to actuator's saturation. These parameters are tuned offline by iteratively minimizing the J_2 to yield the best position-regulation behavior. The selected values are shown in Table 2. The differential-equation solution is computed as follows.

$$K_f(t) = e^{-\boldsymbol{F}t} K_f(0) + \int_0^t \left(e^{-\boldsymbol{F}(t-\tau)} \boldsymbol{G} v(t)\right) d\tau \quad (20)$$

The preset gain vector K_{lqr}, identified in (14), is utilized as the $K_f(0)$ in (20). The control law representing the Fisher-adaptive Self-Tuning-Regulator (F-STR) is given by (21)

$$u(t) = -K_f(t) x(t) \quad (21)$$

Table 2. Tuned parameters of Fisher-adaptive functions

Parameter	Range of selection	Tuned value
γ_α	[0, 1]	0.035
γ_θ	[0, 1]	0.043
$\gamma_{\dot{\alpha}}$	[0, 1]	0.013
$\gamma_{\dot{\theta}}$	[0, 1]	0.021
β_α	[0, 100]	27.4
β_θ	[0, 100]	52.5
$\beta_{\dot{\alpha}}$	[0, 100]	12.6
$\beta_{\dot{\theta}}$	[0, 100]	22.8

The vector $K_f(t)$ yields updated values of the state-feedback gains after every sampling-interval. The asymptotic convergence of the aforementioned adaptive controller is verified via the Lyapunov function shown below.

$$G(e_x) = \frac{1}{2} e_x^2 \quad (22)$$

where, 'x' represents the state-variables being considered (θ or α), and φ is an arbitrary variable. The right-hand side term is clearly positive as it computes the square-of-error in θ or α. Hence, the function $G(e_x)$ is positive. The first-derivative of the Lyapunov function is expressed below.

$$\dot{G} = e_x \dot{e}_x \quad (23)$$

It is well known that in the regulation problem, the reference position has no impact on the controller design. Hence, the state-variable $x(t) = e_x(t)$. The control law dealing with the pendulum angle or the arm angle is thus given by (24).

$$k_{p,x} e_x - k_{d,x} \dot{e}_x = 0 \quad (24)$$

Combining the derivative, $\dot{G}$, with either of these control laws presents the expression in (25).

$$\dot{G} = \left(\frac{k_{d,x}}{k_{p,x}}\right) e_x^2 \quad (25)$$

The expression of $\dot{G}$, shown in (25), will be negative as long as $k_{p,x} < 0$ and $k_{d,x} > 0$. This condition guarantees the stability of the aforementioned adaptive control law. These conditions are also verified via the preset state-feedback gains shown in (14). The "Fisher" adaptation mechanism captures the variations in the magnitude and direction of error-dynamics to improve the system's response-speed and strengthen its damping.

4.2. Nonlinearly-scaled MRAC (N-MRAC)

This section presents the formulation of an original self-tuning LQR augmented with a modified Model-Reference-Adaptive-System (MRAS) (Kavuran et al., 2017). The conventional MRAS automatically updates the gain vector online by minimizing the error between the outputs of the reference model, generated by the LQR, and the actual system (Duka et al., 2007; Saleem et al., 2020b).

Consider the linear system given in (5). It is desired to construct an adaptive control law that is capable of manipulating the angular behavior of the RIP system to imitate the response of the reference model (Chen, 2017). The reference model is given by (26).

$$\dot{x}_{ref}(t) = \boldsymbol{A_{ref}} x_{ref}(t) \quad (26)$$

The linear adaptive control law is given by (27).

$$u(t) = -K_a(t)x(t) \quad (27)$$

where, $K_a(t)$ is the self-tuning gain vector that is dynamically updated via MRAS. The closed-loop representation of the reference and actual system is given in (28) and (29).

$$\dot{x}(t) = (\boldsymbol{A} - \boldsymbol{B}K_a)x(t) \quad (28)$$

$$\dot{x}_{ref}(t) = \left(\boldsymbol{A} - \boldsymbol{B}\widehat{K}_a\right)x_{ref}(t) \quad (29)$$

The error between the reference and the actual states is computed via (30).

$$e(t) = x(t) - x_{ref}(t) \quad (30)$$

The error equation decides the convergence rate of the adaptation mechanism. The time-derivative of the error is given by (31).

$$\dot{e}(t) = \dot{x}(t) - \dot{x}_{ref}(t) = \boldsymbol{A}x(t) + \boldsymbol{B}u(t) - \boldsymbol{A_{ref}} \quad (31)$$

By simultaneously adding and subtracting the term, $\boldsymbol{A_{ref}}x(t)$, on the right-hand side of equation (31), the expression of error-derivative can be simplified according to (32).

$$\dot{e}(t) = \boldsymbol{A_{ref}}e(t) + \boldsymbol{\delta}\left(K_a - \widehat{K}_a\right) \quad (32)$$

such that, $\boldsymbol{\delta} = -\boldsymbol{B}x(t)^T$

It is assumed that the conditions needed for precise model tracking have been completely fulfilled while simplifying the expression of error-derivative. The quadratic Lyapunov function, expressed in (33), is used to develop a stable online gain-adaptation law that modifies the values of K_a after every sampling interval (Hassanzadeh et al., 2011).

$$H(e, K_a) = \frac{1}{2}\left[\boldsymbol{\varphi}e(t)^T\overline{\boldsymbol{P}}e(t) + (K_a - \widehat{K}_a)^T(K_a - \widehat{K}_a)\right] \quad (33)$$

where, $\boldsymbol{\varphi}$ and $\overline{\boldsymbol{P}}$ are both positive definite matrices, whereas, $H(e, K_a)$ is positive semi-definite. The matrix $\boldsymbol{\varphi}$ is referred to as the adaptation-gain matrix. The matrix $\overline{\boldsymbol{P}}$ is calculated offline using the following equation (Cuong et al., 2013).

$$\boldsymbol{A_{ref}^T}\overline{\boldsymbol{P}} + \overline{\boldsymbol{P}}\boldsymbol{A_{ref}} = -\boldsymbol{Q} \quad (34)$$

The $\boldsymbol{Q}$ matrix, identified in (13), is used to solve the equation (34). Following the mathematical property in (34), there would always exist a pair of positive definite matrices, $\overline{\boldsymbol{P}}$ and $\boldsymbol{Q}$, if $\boldsymbol{A_{ref}}$ is stable. The time-derivative of the Lyapunov function is given by (35).

$$\dot{H}(e, K_a) = -\frac{1}{2}\boldsymbol{\varphi}e(t)^T\boldsymbol{Q}e(t) + \left(K_a - \widehat{K}_a\right)^T\left(\dot{K}_a + \boldsymbol{\varphi}\boldsymbol{\delta}^T\overline{\boldsymbol{P}}e(t)\right) \quad (35)$$

For $\dot{H}(e, K_a)$ to be negative-definite, the expression in (36) is chosen as the online gain adjustment law.

$$\dot{K}_a = -\boldsymbol{\varphi}\boldsymbol{\delta}^T\overline{\boldsymbol{P}}e(t) \quad (36)$$

This expression proves that $e(t)$ will eventually converge to zero. The simplified expression of the gain adjustment law is given in (37).

$$\dot{K}_a = \boldsymbol{\varphi}x(t)\boldsymbol{B}^T\overline{\boldsymbol{P}}e(t) \quad (37)$$

The adaptation-gain matrix, $\boldsymbol{\varphi}$, directly influences the convergence-rate and sensitivity of the gain adjustment law. The matrix is given by (38).

$$\boldsymbol{\varphi} = diag(\varphi_\alpha \quad \varphi_\theta \quad \varphi_{\dot{\alpha}} \quad \varphi_{\dot{\theta}}) \quad (38)$$

The dependence of gain-adjustment law on the adaptation-gains, φ_x, varies with respect to the changes occurring in the system's state-dynamics in order to efficiently respond to the state-variations (Saleem at al., 2020). Under perturbed situations, a higher value of adaptation-gain is selected for quick convergence of adaptation-gains due to the rapid variations occurring in the state-dynamics. During steady-state conditions, a lower convergence rate is required to render soft control effort due to the gentle state-variations. A larger adaptation gain during disturbed conditions minimizes the transient recovery times, whereas a smaller adaptation-gain during steady-state conditions damps the steady-state fluctuations (Hassanzadeh et al., 2011). It is evident that preset adaptation-gains lack the flexibility to direct the softness or stiffness of the control-input trajectory under ever-changing state-dynamics (Saleem at al., 2020).

Hence, in this research, a smooth transitioning mechanism is employed that enables the MRAS to automatically commute between different linear optimal controllers, after every sampling interval, to stabilize the RIP under steady-state as wells as the disturbed-state. For this purpose, pre-calibrated nonlinear-scaling functions are employed that smoothly increase the adaptation-gains for large magnitudes of error, and vice versa. The zero-mean Gaussian functions are selected because they are symmetrical, continuous, and bounded (Balestrino et al., 2009). The proposed Gaussian gain-scaling functions are presented as follows.

$$\varphi_\alpha(e_\alpha, t) = \varphi_{\alpha,ds} - \left(\varphi_{\alpha,ds} - \varphi_{\alpha,ss}\right)\exp(-\delta_\alpha|e_\alpha(t)|^2) \quad (39)$$

$$\varphi_\theta(e_\theta, t) = \varphi_{\theta,ds} - \left(\varphi_{\theta,ds} - \varphi_{\theta,ss}\right)\exp(-\delta_\theta|e_\theta(t)|^2) \quad (40)$$

$$\varphi_{\dot{\alpha}}(e_\alpha, t) = \varphi_{\dot{\alpha},ds} - \left(\varphi_{\dot{\alpha},ds} - \varphi_{\dot{\alpha},ss}\right)\exp(-\delta_{\dot{\alpha}}|e_\alpha(t)|^2) \quad (41)$$

$$\varphi_{\dot{\theta}}(e_\theta, t) = \varphi_{\dot{\theta},ds} - \left(\varphi_{\dot{\theta},ds} - \varphi_{\dot{\theta},ss}\right)\exp(-\delta_{\dot{\theta}}|e_\theta(t)|^2) \quad (42)$$

where, exp(.) is an exponential functions, δ_x are pre-fixed variation-rates of the Gaussian scaling functions associated with the respective state-variables. The parameters $\varphi_{x,ss}$ and $\varphi_{x,ss}$ represent the adaptation-gains associated with the steady-state and the disturbed-state of RIP, respectively. The variation-rates are tuned by iteratively minimizing the cost function J_2 to deliver a time-optimal control effort. The range-space and the optimized value of each parameter are provided in Table 3. The values of $\varphi_{x,ss}$ and $\varphi_{x,ss}$ are selected in accordance with the research findings presented in (Hassanzadeh et al., 2011). The upper and lower limits of each adaptation-gain function are recorded in Table 4. The waveform of the adaptation-gain function is shown in Figure 3. The augmentation of MRAS with self-adjusting adaptation-gains allows the controller to flexibly compensate the effects of abrupt dynamic changes as the system transits from disturbed-state to steady-state, and vice-versa. The self-adjusting adaptation-gain matrix is presented in (43).

$$\overline{\boldsymbol{\varphi}} = diag(\varphi_\alpha(e_\alpha, t) \quad \varphi_\theta(e_\theta, t) \quad \varphi_{\dot\alpha}(e_\alpha, t) \quad \varphi_{\dot\theta}(e_\theta, t)) \qquad (43)$$

The modified online gain adjustment law is presented in (44).

$$\dot{\overline{K}}_a = \overline{\boldsymbol{\varphi}} x(t)\boldsymbol{B}^T\overline{\boldsymbol{P}}e(t) \qquad (44)$$

The numerical integration of the gain adjustment law in (44) provides the following expression for the online adaptive modulation of the state-feedback gains.

$$\overline{K}_a(t) = \overline{K}_a(0) + \int_0^t \left(\overline{\boldsymbol{\varphi}} x(t)\boldsymbol{B}^T\overline{\boldsymbol{P}}e(t)\right) d\tau \qquad (45)$$

The fixed-gain vector K_{lqr}, identified in (14), is utilized as the $\overline{K}_a(0)$ in (45). The Nonlinearly-scaled MRAC (N-MRAC) law is expressed in (46).

$$u(t) = \overline{K}_a(t)x(t) \qquad (46)$$

where, $\overline{K}_a(t) = -[\bar{k}_\alpha(t) \quad \bar{k}_\theta(t) \quad \bar{k}_{\dot\alpha}(t) \quad \bar{k}_{\dot\theta}(t)]$

The block diagram of the N-MRAC is shown in Figure 4.

Table 3. Selected variances of the Gaussian functions

Parameter	Range of selection	Tuned value
δ_α	[0, 100]	26.5
δ_θ	[0, 100]	32.7
$\delta_{\dot\alpha}$	[0, 100]	42.1
$\delta_{\dot\theta}$	[0, 100]	45.3

Table 4. Limits of adaptation-gains for N-MRAC

State	Disturbed-state				Steady-state			
Limit	$\varphi_{\alpha,ds}$	$\varphi_{\theta,ds}$	$\varphi_{\dot\alpha,ds}$	$\varphi_{\dot\theta,ds}$	$\varphi_{\alpha,ss}$	$\varphi_{\theta,ss}$	$\varphi_{\dot\alpha,ss}$	$\varphi_{\dot\theta,ss}$
Value	2	1	3	2	1	0.1	0.2	0.1

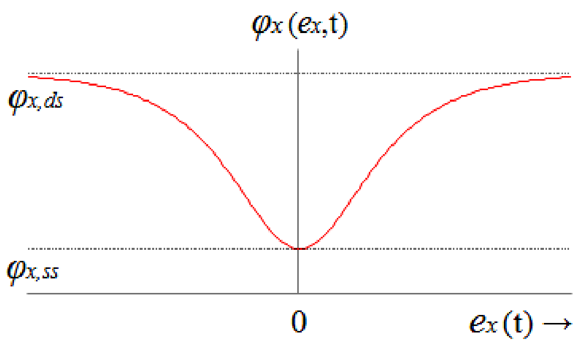

Figure 3. The waveform of the adaptation-gain functions

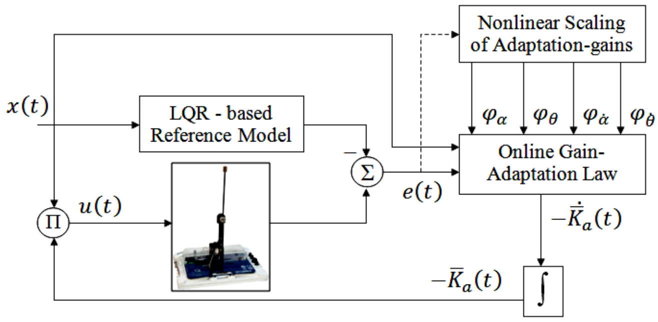

Figure 4. The block diagram of the N-MRAC scheme

5. EXPERIMENTAL SETUP

This section presents a detailed experimental evaluation of the proposed adaptive control strategies via hardware-in-the-loop experiments conducted on the QNET RIP setup [28].

5.1. Experimental Evaluation

The details of the experimental setup have already been discussed in Section 2. The performance of N-MRAC is compared with the fixed-gain LQR and F-STR via four unique test-cases. The test-cases analyze the position-regulation, disturbance-rejection, random noise attenuation, and modeling-error compensation capability of each of the aforementioned controllers. To simplify the visualization, the angular responses are deliberately shown in degrees (deg.).

A. Position-regulation behavior: This test case examines the system's position-regulation behavior. The objective is to vertically stabilize the pendulum rod with minimum deviations while making sure that the arm tracks its initial position. The position-regulation response and the corresponding control input profile of each controller are graphically illustrated in Figures 5, 6, and 7, respectively.

B. Impulsive-disturbance rejection: The robustness of proposed controllers against exogenous disturbances is examined by injected a pulse in the control input at t ≈ 1.5 s. The magnitude and duration of the applied pulse are -10.0 V and 0.1 ms, respectively. The time-domain behavior of each controller is illustrated in Figures 8, 9, and 10, respectively.

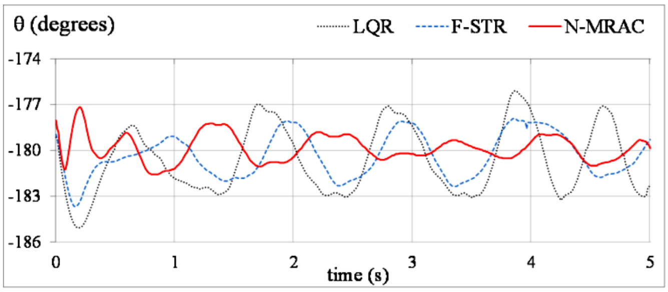

Figure 5. Pendulum angle response under normal conditions

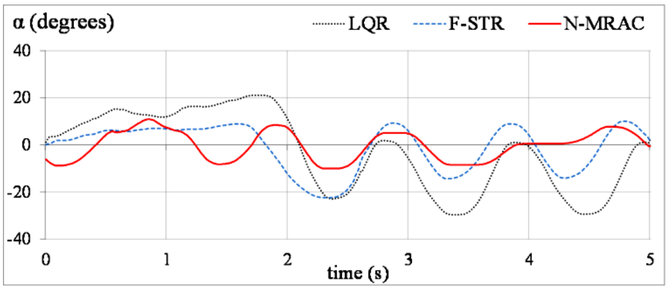

Figure 6. Arm angle response under normal conditions

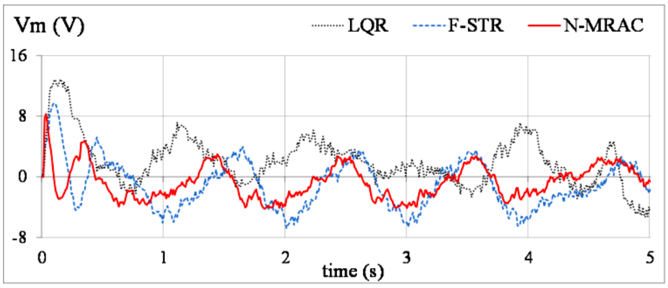

Figure 7. Control voltage response under normal conditions

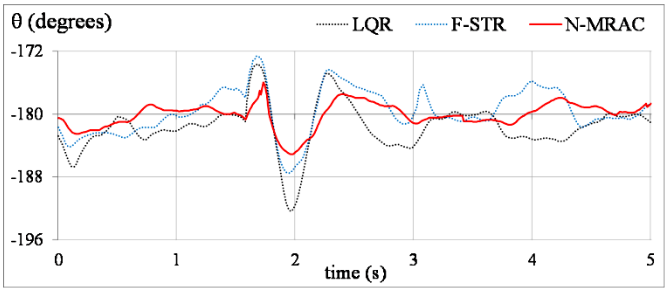

Figure 8. Pendulum angle response under pulse disturbance

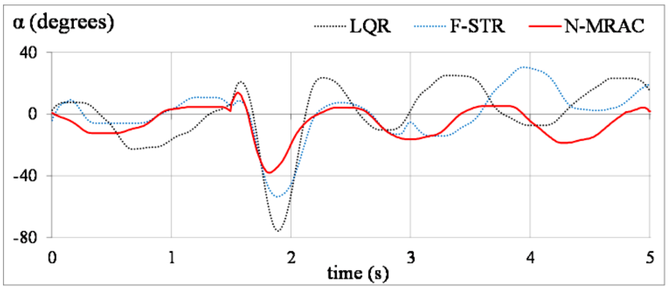

Figure 9. Arm angle response under pulse disturbance

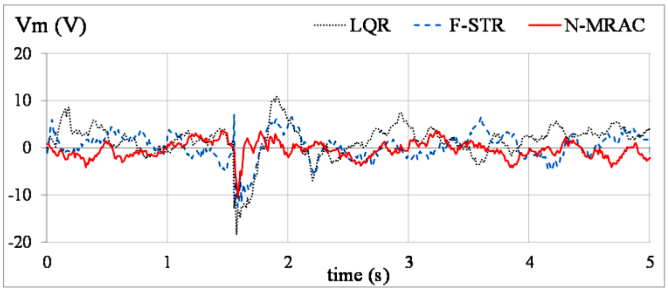

Figure 10. Control voltage response under pulse disturbance

C. Noise attenuation: The controller's immunity against the detrimental effects of measurement noise (or mechanical vibrations) is evaluated by adding a bounded white noise signal in the control input. The injected signal has a signal-to-noise ratio of +20.0 dB. The resulting fluctuations observed in the time-domain response of each controller are depicted in Figures 11, 12, and 13, respectively.

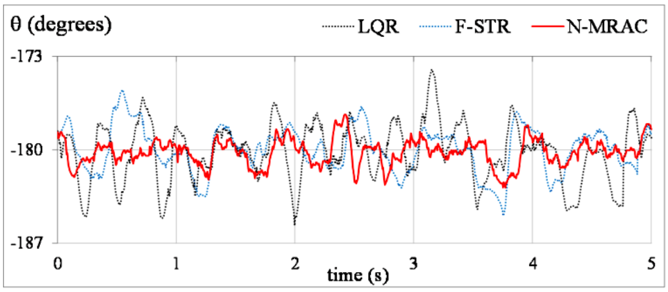

Figure 11. Pendulum angle response under white noise

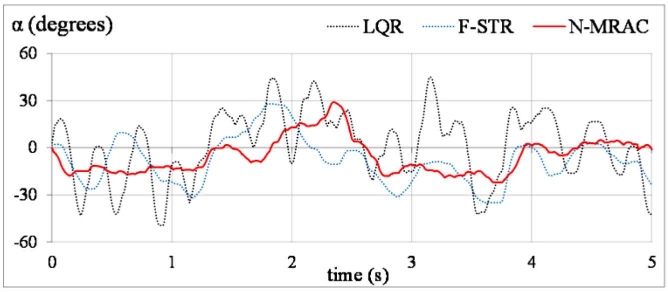

Figure 12. Arm angle response under white noise

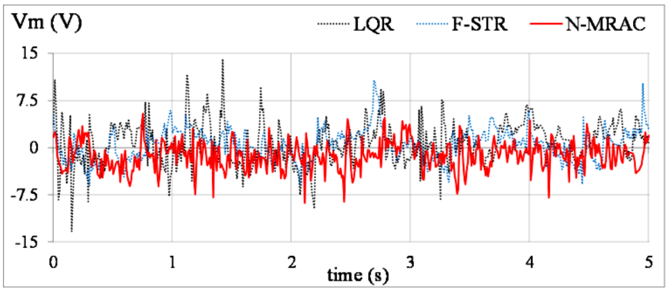

Figure 13. Control voltage response under white noise

D. Modeling-error compensation: The controller's immunity against modeling-errors is assessed by introducing a step-increment in R_m via the mechanism shown in Figure 13. Initially, the RIP is balanced under nominal conditions. At t ≈ 1.5 s, a 1.0 Ω resistor is connected in series with the motor terminals by changing the position of the selector-switch, shown in Figure 14, from A to B. The resulting state and control input variations of each controller are graphically illustrated in Figures 15, 16, and 17, respectively.

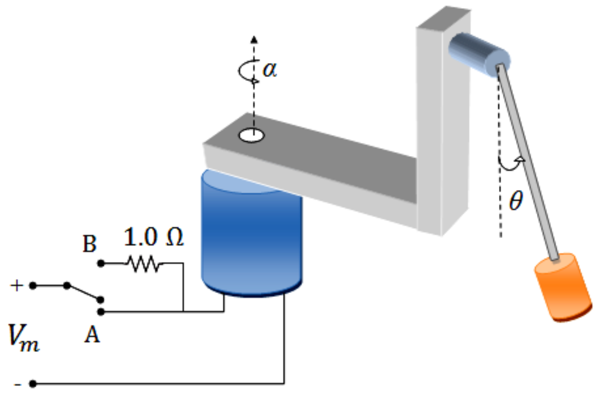

Figure 14. Schematic of the modified RIP setup

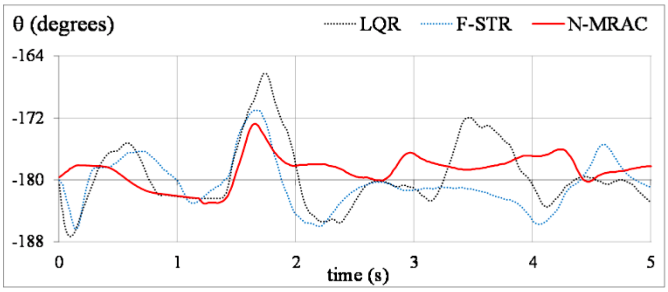

Figure 15. Pendulum angle response under modeling-error

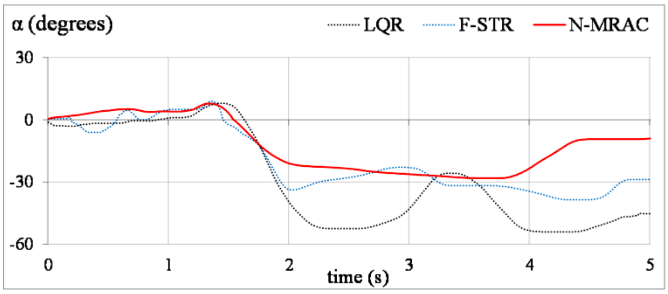

Figure 16. Arm angle response under modeling-error

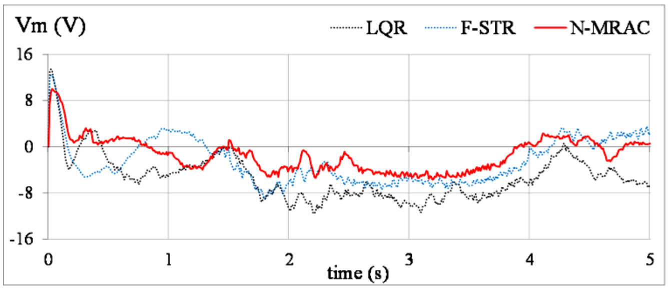

Figure 17. Control voltage response under modeling-error

5.2. Analysis and Discussions

The performance analysis is done in terms of the root-mean-squared value of state-error ($RMSE_x$) in degrees, the absolute value of peak overshoot or undershoots ($M_{p,x}$) under transient disturbances, the time taken by the response to settle within ±2% of the reference value ($t_{s,x}$), the average control power evaluated in terms of mean-squared-value of the motor control voltage (MSV_m), and the peak control voltage ($V_{m,p}$) in the control profile under transient disturbances. The comparative performance assessment of the experimental results is summarized in Table 5. The results clearly validate the superior robustness and time-optimality of the N-MRAC against parametric uncertainness, bounded exogenous disturbances, and modeling errors.

In Test-A, the angular responses of LQR exhibit persistent fluctuations around the reference angles. The angular responses of F-STR converge relatively faster to reference than the LQR, with a relatively lesser amplitude of oscillations in the equilibrium position. The N-MRAC exhibits the most time-optimal control effort. The arm- and rod-angle quickly converge to the reference angles and track them with minimal steady-state fluctuations. In Test-B, the N-MRAC response exhibits rapid transits with reasonable damping to compensate for the effects of impulsive disturbances. The N-MRAC demonstrates the minimum magnitude of M_p as well as t_{rec} after recovering from the transient disturbance. In Test-C, the arm and rod vibrate persistently throughout the trial when the system is equipped with LQR. The responses yielded by F-STR also exhibit persistent oscillations throughout the time-window with a relatively lesser magnitude of RMSE. The N-MRAC effectively attenuates the influence of noise signal and manifests minimum RMSE magnitudes in the angular responses of arm and pendulum.

Table 5. Summary of experimental results

Test	Characteristic	Controllers		
		LQR	**F-STR**	**N-MRAC**
A	$RMSE_\theta$ (deg.)	2.31	1.46	0.88
	$RMSE_\alpha$ (deg.)	16.61	9.76	6.13
	MSV_m (V^2)	14.97	10.14	5.33
B	$RMSE_\theta$ (deg.)	3.42	2.92	1.60
	$\lvert M_{p,\theta}\rvert$ (deg.)	12.03	7.51	5.12
	$t_{s,\theta}$ (s)	1.55	1.26	1.21
	$RMSE_\alpha$ (deg.)	20.84	16.68	11.87
	$\lvert M_{p,\alpha}\rvert$ (deg.)	75.86	53.66	38.02
	$t_{s,\alpha}$ (s)	1.54	1.19	1.15
	MSV_m (V^2)	15.42	8.63	4.70
	$V_{m,p}$ (V)	-18.42	-12.61	-10.70
C	$RMSE_\theta$ (deg.)	2.21	1.76	1.02
	$RMSE_\alpha$ (deg.)	19.56	17.47	11.44
	MSV_m (V^2)	13.83	10.17	6.72
D	$RMSE_\theta$ (deg.)	4.38	3.30	2.35
	$RMSE_\alpha$ (deg.)	36.58	25.09	17.84
	MSV_m (V^2)	40.17	21.66	10.56

In Test-D, the N-MRAC robustly compensates for the modeling-error. It overcomes the detrimental effects of the induced parametric variations in minimum time while effectively damping the fluctuations around the reference angle.

The superior disturbance-rejection capability exhibited by N-MRAC is attributed to the enhanced adaptability of the state-feedback gains, rendered by the self-adjusting adaptation-gains in the MRAS law. This arrangement significantly improves the response-speed of the controller and efficiently compensates the detrimental effects of bounded exogenous disturbances and parametric variations.

6. CONCLUSION

This paper presents the systematic formulation of an enhanced adaptive-optimal stabilization control strategy for RIP systems by employing a resilient state-error-dependent self-tuning mechanism. Two online self-adaptive strategies are comparatively analyzed; namely, the Fisher-adaptive gain-adjustment law as well as nonlinearly-scaled MRAS. Each online gain-adjustment mechanism is methodically synthesized and then retrofitted with the baseline LQR. The F-STR reasonably mitigates the effects of external disturbances and modeling-errors encountered by the system. However, to further enhance the controller's adaptability and robustness against nonlinear disturbances, a modified MRAC is employed. The adaptation-gain matrix of the gain-adjustment law in MRAC is dynamically modified via pre-configured state-error dependent Gaussian scaling functions. The mutation of MRAS via smooth nonlinear scaling functions considerably improves the pendulum's error convergence-rate and strengthens its damping against fluctuations. The superior robustness of N-MRAC is validated by conducting credible experiments on QNET Rotary Pendulum Board and analyzing the corresponding results in comparison with other controller variants. There is plenty of room for future enhancements. The robustness of the proposed control strategy can be investigated by applying it to control other electro-mechanical systems. Moreover, indirect hierarchical adaptive control strategies can be examined for the online modification of the state-feedback controller gains to ensure improved stabilization of self-balancing electro-mechanical systems.

REFERENCES

Ashrafiuon, H., and Whitman, A.M. (2011). Closed-loop dynamic analysis of a rotary inverted pendulum for control design. *Journal of Dynamic Systems, Measurement, and Control*, 134(2), pp. 1-9.

Balamurugan, S., Venkatesh, P., and Varatharajan, M. (2017). Fuzzy sliding-mode control with low pass filter to reduce chattering effect: an experimental validation on Quanser SRIP. *Sadhana*, 42(10), pp. 1693–1703.

Balestrino, A., Biagini, V., Bolognesi, P., and Crisostomi, E. (2009). Advanced Variable Structure PI controllers. In: *Proceedings of IEEE Conference on Emerging Technologies & Factory Automation*, Mallorca, Spain, 22-25 September 2009, pp. 1-8.

Balestrino, A., Caiti, A., Calabr, V., Crisostomi, E., and Landi, A. (2011). *Chaper 5 - From Basic to Advanced PI Controllers: A Complexity vs. Performance Comparison* In: Advances in PID Control, V.D. Yurkevich (Ed.), Intech, Rijeka, Croatia, pp. 85–100.

Batmani, Y., Davoodi, M., and Meskin, N. (2017). Nonlinear Suboptimal Tracking Controller Design Using State-Dependent Riccati Equation Technique. *IEEE Transactions on Control System Technology*, 25(5), pp. 1833-1839.

Bernat, J., and Stepien, S. (2012). The study on the model reference adaptive control with proportional derivative action. International Journal of Control, 85(6), pp. 765–778.

Bhatti, O.S., Mehmood-ul-Hasan, K., and Imtiaz, M.A. (2015). Attitude Control and Stabilization of a Two-Wheeled Self-Balancing Robot. *Control Engineering and Applied Informatics*, 17(3), pp. 98-104.

Bhatti, O.S., Tariq, O.S., Manzar, A., and Khan, O.A. (2018). Adaptive intelligent cascade control of a ball-riding robot for optimal balancing and station-keeping. *Advanced Robotics*, 32(2), pp. 63-76

Blanchini, F., Parisini, T., Pellegrino, F.A., and Pin, G. (2009). High-gain adaptive control: a derivative-based approach. *IEEE Transactions on Automic Control*, 54(9), pp. 2164–2169.

Boubaker, O. (2013). The inverted pendulum benchmark in nonlinear control theory: a survey. *International Journal of Advanced Robotic Systems*, 10(5), pp. 233–242.

Chen, K.Y. (2017). Model reference adaptive minimum-energy control for a mechatronic elevator system, Optimal Control Applications and Methods, 38(1), pp. 3–18.

Cuong, N.D., Lanh, N.V., and Huyen, D.V. (2013). Design of MRAS-based adaptive control systems, In: *Proceedings of International Conference on Control, Automation and Information Sciences*, Nha Trang, Vietnam, 25-28 Nov. 2013, pp. 79-84.

Duka, A.D., Oltean, S.E., and Dulău, M. (2007). Model reference adaptive vs. learning control for the inverted pendulum. A comparative case study. *Control Engineering and Applied Informatics*, 9(4), pp. 67-75.

Fisher, A.D. VanZwieten, J.H., and VanZwieten, T.S. (2009). Adaptive Control of Small Outboard-Powered Boats for Survey Applications. In: *OCEANS'09 Proceedings of the MTS/IEEE Marine Technology for Our Future: Global and Local Challenges*, Biloxi, Mississippi, 26-29 October 2009, pp. 1-9.

Ghartemani, M.K., Khajehoddin, S.A., Jain, P., Bakhshai, A. (2011). Linear quadratic output tracking and disturbance rejection. *International Journal of Control*, 84(8), pp. 1442-1449.

Gritli, H., and Belghit, S. (2018). Robust feedback control of the underactuated Inertia Wheel Inverted Pendulum under parametric uncertainties and subject to external disturbances: LMI formulation. *Journal of Franklin Institute*, 355(18), pp. 9150-9191.

Hanwate, S., Hote, Y.V., and Budhraja, A. (2019). Design and implementation of adaptive control logic for cart-inverted pendulum system. *Proceedings of the Institute*

of Mechanical Engineers, Part I: Journal of Systems and Control Engineering*, 233(2), pp. 164-178.
Hassanzadeh, A., Nejadfard, A., and Zadi, M. (2011). A Multivariable Adaptive Control Approach for Stabilization of a Cart-Type Double Inverted Pendulum. *Mathematical Problems in Engineering*, 2011, Article ID 970786.
Kavuran, G., Ates, A., Alagoz, B.B., and Yeroglu, C. (2017). An Experimental Study on Model Reference Adaptive Control of TRMS by Error-Modified Fractional Order MIT Rule. *Control Engineering and Applied Informatics*, 19(4), pp. 101-111.
Li, Z., Yang, C., and Fan, L. (2013). *Advanced Control of Wheeled Inverted Pendulum Systems*. Springer, London.
Lewis, F.L., Vrabie, D., and Syrmos, V.L. (2012). *Optimal Control*. John Wiley and Sons, New Jersey.
Mahmoud, M.S. (2018). *Advanced Control Design with Application to Electromechanical Systems*. 1st Ed., Elsevier Science, New York.
Prasad, L.B., Tyagi, B., and Gupta, H.A. (2014). Optimal Control of Nonlinear Inverted Pendulum System Using PID Controller and LQR: Performance Analysis Without and With Disturbance Input. *International Journal of Automation and Computing*, 11(6), pp. 661–670.
Saleem, O., Hassan, H., Khan, A., and Javaid, U. (2017). Adaptive Fuzzy-PD Tracking Controller for Optimal Visual-Servoing of Wheeled Mobile Robots. *Control Engineering and Applied Informatics*, 19(3), pp. 58-68.
Saleem, O., Rizwan, M., Ahmad, M. (2018). Augmented linear quadratic tracker for enhanced output-voltage control of DC-DC buck converter. *Control Engineering and Applied Informatics*, 20(4), pp. 40-49.
Saleem, O., Abbas, F., Khan, M.U., Imtiaz, M.A., and Khalid, S. (2018). Adaptive Collaborative Position Control of a Tendon-Driven Robotic Finger. *Control Engineering and Applied Informatics*, 20(2), pp. 87-99.
Saleem, O., Rizwan, M., Shiokolas, P.S., and Ali, B. (2019). Genetically Optimized ANFIS-based PID Controller Design for Posture-Stabilization of Self-Balancing-Robots under Depleting Battery Conditions. *Control Engineering and Applied Informatics*, 21(4), pp. 22-33.
Saleem, O., Shami, U.T., Mahmood-ul-Hasan, K., Abbas, F., and Mahmood, S. (2019). Robust-Optimal Output-Voltage Control of Buck Converter using Fuzzy Adaptive Weighted Combination of Linear Feedback Controllers. *Control Engineering and Applied Informatics*, 21(2), pp. 43-53.
Saleem, O., and Mahmood-ul-Hasan, K. (2019). Robust stabilisation of rotary inverted pendulum using intelligently optimised nonlinear self-adaptive dual fractional order PD controllers. *International Journal of Systems Science*, 50(7), pp. 1399-1414.
Saleem, O., and Rizwan, M. (2019). Performance optimization of LQR-based PID controller for DC-DC buck converter via iterative-learning-tuning of state-weighting matrix. *International Journal of Numerical Modelling*, 32, e2572.
Saleem, O., Rizwan, M., Mahmood-ul-Hasan, K., and Ahmad, M. (2020). Performance enhancement of multivariable model-reference optimal adaptive motor speed controller using error-dependent hyperbolic gain functions. *Automatika*, 61(1), pp. 117-131.
Saleem, O., Mahmood-ul-Hasan, K., and Rizwan, M. (2020). Self-Tuning State-Feedback Control of Rotary Pendulum via Online Adaptive Reconfiguration of Control Penalty-Factor. *Control Engineering and Applied Informatics*, 22(4), pp. 23-33.
Subramaniana, R.G., and Elumalai, V.K. (2016). Robust MRAC augmented baseline LQR for tracking control of 2 DoF helicopter. *Robotics and Autonomous Systems*, 86, pp. 70–77.
Sukontanakarn, V., and Parnichkun, M. (2009). Real-Time Optimal Control for Rotary Inverted Pendulum, *American Journal of Applied Sciences*, 6(6), pp. 1106-1115.
Szuster, M., and Hendzel, Z. (2017). *Intelligent optimal adaptive control for mechatronic systems, Studies in Systems, Decision and Control*. Springer, Berlin, Germany.
Yu, H. Liu, Y., and Yang, T. (2008). Closed-loop tracking control of a pendulum-driven cart-pole underactuated system, *Proceedings of the Institute of Mechanical Engineers, Part I: Journal of Systems and Control Engineering*, 222(2), pp. 109–125.
Zhang, H., Wang, J., and Lu, G. (2014). Self-organizing fuzzy optimal control for under-actuated systems. *Proceedings of the Institute of Mechanical Engineers, Part I: Journal of Systems and Control Engineering*, 228(8), pp. 578-590.